

Efficient Implementation of MPC-based AGC for Real-World Systems with Low Inertia

Paul Mc Namara^a, Federico Milano^{a,*}

^a*University College Dublin, Belfield, Dublin 4, Ireland*

Abstract

The paper discusses practical implementation and computational aspects of an AGC scheme based on model predictive control (MPC) for a real-world power system, namely the all-island Irish transmission system. This system is particularly interesting from the frequency regulation point of view due to the high penetration of wind power generation. This leads to a significant reduction in system inertia, which in turn impacts on the ability of the system operator to regulate the system frequency. The paper compares the performance of the MPC-based AGC with a conventional AGC based on PI controllers and draws relevant conclusions. The case study is a high-resolution simulation of a 1,479-bus model of the Irish electrical grid with significant wind penetration, stochastic loads, and controller delays.

Keywords: Automatic Generation Control, Model Predictive Control, PI control, Wind Generation

1. Introduction

1.1. Motivation

Current implementations of primary and secondary frequency regulation of power systems rely on the inertia of synchronous machines and control characteristics of conventional power plants [1]. As renewable penetration levels increase

*Corresponding author

Email address: federico.milano@ucd.ie (Federico Milano)

in grids, tight frequency regulation becomes increasingly difficult [2, 3]. While primary control gains are typically designed to be fixed and local in nature, secondary control algorithms are capable of using global system information to determine the control inputs to send to generators. By improving control
10 coordination mechanisms it is possible to improve frequency regulation.

Model predictive control (MPC) appears as a promising technique to improve frequency control and has been considered in recent years in several studies [4, 9, 10, 11, 12, 15, 16, 17, 18]. However, computational and implementation issues related to MPC have often been pointed to as the most serious constraint
15 facing its practical implementation. As a matter of fact, the current literature only considers small- and medium-size cases studies. This paper deals with an efficient and realistic implementation of an MPC-based AGC and considers a real-world power system, namely a 1,479-bus model of the all-island Irish transmission grid, with a high penetration (up to 55%) of non-synchronous
20 generation.

1.2. Literature Review

Model Predictive Control (MPC) is a MIMO optimization based control technique that uses state-space predictions in order to formulate optimal inputs to a system. MPC is a mature technology at this stage having originally been
25 developed in the 1980s. It is used in a widespread fashion in the process industry and is available in a number of commercial packages such as ABB's 3dMPC, AspenTech's Dynamic Matrix Control (DMC), and Pavilion Technologies Inc.'s Process Perfecter products [6]. In recent years many researchers have considered power systems control in an optimal control framework [7, 8]. MPC has
30 been applied previously for centralised [4, 9, 10, 11, 12, 13], hierarchical [14], and non-centralised [15, 16, 17, 19] control in power systems for AGC and other applications. It has been shown to offer improved frequency regulation performance and robustness to uncertainty when compared to standard PI control [4, 20].

35 When states are not measurable for use in MPC, they can be estimated

using an optimal state estimator called a Kalman filter. Kalman filtering is also a mature technology at this stage having originally been developed by Kalman and Bucy in the 1960s. It is used for a wide variety of applications in industry, most famously being used by NASA as part of the Apollo project to aid the
40 navigation of manned spacecraft going to the moon and back [21]. A range of Kalman filters have been proposed for power system state estimation [22, 23, 24].

One of the main issues with most implementations of MPC for power systems control is the scale and realism of the power system considered. Typically relatively small scale power systems with less than 50 buses are considered, and
45 the power systems used for studies are usually not derived from real life grid configurations. There are a number of notable exceptions in the literature. MPC has been used to control Voltage Source Converter based devices embedded in models of the European and British grids in [11] and [25], respectively.

Advanced MPC control strategies were used for applying distributed voltage
50 control and centralized AGC to the Nordic 23-generator system model in [12] and [9]. In [26] advanced MPC is used to penalise deviations from dispatch setpoints considering a range of constraints, and is applied to a large scale model of the Californian system. It should be noted that while [9] considers transient dynamics, only the long term thermal line dynamics are considered in
55 [26], with the remaining variables considered at a linearised power flow level.

1.3. Open Challenges with MPC for AGC

1.3.1. AGC for low-inertia systems

As synchronous machines are replaced in power systems, and there is a consequent decrease in system inertia and increase in generation uncertainty, tight
60 frequency regulation becomes more difficult. Thus, it is of interest to investigate the performance of MPC for AGC in large-scale realistic power systems with large renewable penetrations, and low levels of system inertia. This, in turn, would provide evidence as to whether MPC could aid in allowing larger penetrations of renewable sources on grids, when compared to standard PI approaches.

65 *1.3.2. Practical implementation of MPC-based AGC*

While [9] illustrates the application of state-of-the-art control techniques for AGC, the authors are skeptical as to how such state-of-the-art techniques would be accepted in industry. Given the conservativeness of practitioners in the power systems industry, if MPC were to be used in industry, it is hard to imagine that
70 such complex versions of MPC would be initially embraced, given that simple PI or manual control is used in practice for AGC in most power systems today. It is also desirable in lower inertia grids with small time constants that the control would be computed efficiently. Simple, linear MPC using Kalman filtering for state estimation can be computed in a highly efficient manner and so it is of
75 interest to see how well these algorithms perform in achieving control of the system.

1.3.3. Fast prototyping of MPC-based control schemes

Another barrier to practitioners as regards evaluating the performance of MPC for power systems control is that, to the best of the authors' knowledge,
80 there is no power systems simulation package currently available that provides an integrated MPC toolbox. Given the recent popularity of MPC for use in power systems, and that the setup of MPC controllers involves significantly more effort than that associated with PI controllers, it is desirable that integrated MPC functionality would be incorporated into power systems simulation
85 packages. In turn this could significantly improve the efficiency with which MPC can be set up for evaluating the application of MPC for power systems control.

1.4. Contributions

The paper deals with the three challenges discussed above. The main contributions of the paper are as follows.

- 90 • A discussion on an efficient implementation of MPC for real-world grids with low levels of inertia and a large stochastic renewables penetration. With this aim, a 1,479-bus model of the Irish transmission system is utilised in the case study.

- 95
 • A discussion on practical implementation aspects of the MPC-based AGC scheme, including an efficient Kalman filtering approach for state estimation. The Kalman filter is based on measurements of the individual generator frequency and rotor position. Using modern PMUs and communication systems, it is increasingly possible for TSOs to attain such measurements. A comparison of the performance of MPC-based and conventional PI-based AGC schemes is also provided.
- 100
 • An MPC software implementation based exclusively on state-of-art mathematical libraries, such as Gurobi and SuiteSparse. The MPC toolbox is then integrated in the Dome simulation package [27]. The authors believe that the developed software tool can greatly help with the fast prototyping of MPC-based control techniques for power systems applications and are
- 105
 happy to share the code with the interested readers.

1.5. Organization

110
 The rest of the paper is constructed as follows: Section 2 outlines the power system modelling, focusing in particular on the synchronous generators that are used for AGC. In Section 3, the MPC and Kalman filtering approaches used in this paper are explained. Then, in Section 4, the way in which MPC is applied for AGC is given. The results of the simulations comparing the PI and MPC approaches when used for AGC on the Irish grid are given in Section 5. Finally, in Section 6 conclusions are drawn based on the results of the paper.

115 2. Power system modelling for simulation

Various load, synchronous generator, turbine, wind turbine models, etc., are used in this paper. Full details of the dynamics of all these models can be found in [28]. Due to space constraints in depth details of all of these models are not documented here.

120
 Wind turbines provide the source of stochastic power production in this paper. Wind speeds are modelled using a Weibull distribution, where a Rayleigh

distribution is used to model time variations in wind speed. The test case considered in this paper is the Irish grid. The Weibull distribution is used here based on the accuracy with which Irish wind speeds were described previously using this distribution [29]. However, care should be taken to ensure that suitable wind distributions are applied to different grids. For example, wind power variability was found to have a Laplacian distribution in some North American power systems in [30]. Two types of wind turbines models are used: Constant Speed and Doubly Fed Induction Generator Wind Turbines (CSWT and DFIG, respectively). The CSWT is described by a 5th-order squirrel-cage induction generator model, a turbine model without pitch control, a single-mass shaft model with tower-shadow effect, and a static capacitor bank. The DFIG is a variable-speed wind turbine described by a 5th-order doubly-fed induction generator model, a double-mass elastic shaft model with tower-shadow effect, a turbine model with continuous pitch control, a cubic maximum power point tracking approximation, a first-order Automatic Voltage Regulator (AVR) model, and a converter active power controller. When loads are deterministic, constant PQ models are used in simulations. For the cases involving stochastic PQ loads, Ornstein-Uhlenbeck processes are then used to model the loads [31].

The synchronous generator model is documented in detail in the following, as the controllers in this paper are used to control synchronous generators and so it is directly relevant to the design of the control system. A 6th order dynamic model is used to capture the relevant dynamics of the synchronous generator for simulation purposes as follows:

$$\dot{\delta} = \Omega_b(\omega - \omega_s), \quad (1)$$

$$2H\dot{\omega} = (\tau_m - \tau_e - D(\omega - \omega_s)), \quad (2)$$

$$T'_{d0}\dot{e}'_q - \tilde{T}''_{d0}\dot{\psi}''_d = -e'_q - (x_d - x'_d)i_d + v_f, \quad (3)$$

$$T'_{q0}\dot{e}'_d - \tilde{T}''_{q0}\dot{\psi}''_q = -e'_d + (x_q - x'_q)i_q, \quad (4)$$

$$T''_{d0}\dot{\psi}''_d = -\psi''_d + e'_q - (x'_d - x_\ell)i_d, \quad (5)$$

$$T''_{q0}\dot{\psi}''_q = -\psi''_q - e'_d - (x'_q - x_\ell)i_q, \quad (6)$$

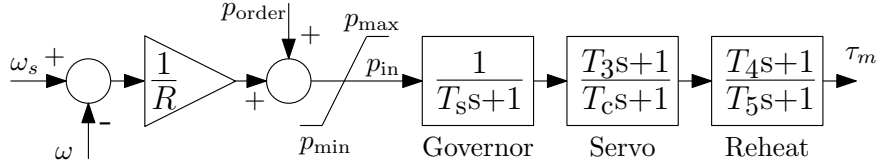


Figure 1: Turbine Governor control diagram [28].

coupled with the following algebraic equations:

$$\tau_e = \psi_d i_q - \psi_q i_d, \quad (7)$$

$$0 = r_a i_d + \psi_q + v_d, \quad (8)$$

$$0 = r_a i_q + \psi_d + v_q, \quad (9)$$

$$0 = \psi_d + x_d'' i_d - \gamma_{d1} e_q' - (1 - \gamma_{d1}) \psi_d'', \quad (10)$$

$$0 = \psi_q + x_q'' i_q - \gamma_{q1} e_d' - (1 - \gamma_{q1}) \psi_q''. \quad (11)$$

140 The authors refer to [28] for definitions of the various system parameters.

The mechanical power is generated using a turbine governor [28], as given in Fig. 1. This consists of a primary frequency controller, designed to control frequency variations instantaneously based on local frequency measurements, and an additional set point p_{order} which allows the elimination of longer term
145 frequency offsets. Voltage regulation is conducted using the AVR and PSS modules as documented in [32, 28].

Traditionally PI controllers have been used to perform AGC. While primary control acts on the local generator frequency signal to regulate the power generated over short ms to s time scales, AGC acts on the s to tens of s scale using global system information to eliminate long term offsets, which result from local primary control using only proportional gains. Using PI for AGC, the Centre of Inertia (COI) frequency signal is sent to a proportional and integral controller to generate $p_{\text{order}}^{\text{coi}}(t)$ as follows [32]:

$$p_{\text{order}}^{\text{coi}}(t) = k_I \int_{t=0}^{t=\infty} \omega_{\text{COI}}(t) - \omega_s \, dt \quad (12)$$

where k_I is the integral gain and the centre of inertia frequency ω_{COI} is given by:

$$\omega_{\text{COI}}(t) = \frac{1}{H_T} \sum_{i=1}^n H_i \omega_i(t) \quad (13)$$

where there are n synchronous generators in the system and $H_T = \sum_{i=1}^n H_i$. Each generator is then assigned its local set point $p_{\text{order}i} = \beta_i p_{\text{order}}^{\text{COI}}$, where β_i is the participation factor for generator i and $\sum_{i=1}^n \beta_i = 1$. In order to implement AGC, it is necessary for the TSO to measure $\omega_{\text{COI}}(t)$, calculate the power to inject into the system, and then communicate the various set points to each of the generators. Thus communication delays occur between the measurement of the frequency and the point at which generators receive the updated set point changes.

3. Model Predictive Control and Kalman filtering

3.1. Model Predictive Control

Model Predictive Control is an optimization based control technique that uses state-space based predictions in order to form optimal inputs to a system over a prediction horizon. While inputs are calculated over the full prediction horizon, only the input for the first sample step of the prediction horizon is applied to the system, and this process is repeated every sample step.

A discrete-time, linear, time-invariant state-space model for a system is given by

$$\mathbf{x}(k+1) = \mathbf{A}\mathbf{x}(k) + \mathbf{B}\mathbf{u}(k) + \mathbf{D}\mathbf{d}(k) + \mathbf{w}(k) \quad (14)$$

$$\mathbf{y}(k) = \mathbf{C}\mathbf{x}(k), \quad (15)$$

where $\mathbf{x}(k)$, $\mathbf{u}(k)$, $\mathbf{d}(k)$, and $\mathbf{y}(k)$ are the states, inputs, disturbances, and outputs of the system at sample step k , respectively. Matrices \mathbf{A} , \mathbf{B} , \mathbf{D} , and \mathbf{C} are the relevant state-space matrices. Vector $\mathbf{w}(k)$ is the process noise vector which is assumed to be drawn from a zero mean multivariate normal distribution with variance $\boldsymbol{\sigma}_w$, i.e., $\mathbf{w}(k) \sim \mathcal{N}(0, \boldsymbol{\sigma}_w)$.

An augmented state-space model allows these equations to be framed in terms of $\Delta \mathbf{u}(k)$, which ensures integral action in the MPC controller. This is given as follows:

$$\boldsymbol{\chi}(k+1) = \overbrace{\begin{bmatrix} \mathbf{A} & \mathbf{0} & \mathbf{D} \\ \mathbf{A} & \mathbf{I} & \mathbf{D} \\ \mathbf{0} & \mathbf{0} & \mathbf{I} \end{bmatrix}}^{\hat{\mathbf{A}}} \boldsymbol{\chi}(k) + \overbrace{\begin{bmatrix} \mathbf{B} \\ \mathbf{B} \\ \mathbf{0} \end{bmatrix}}^{\hat{\mathbf{B}}} \Delta \mathbf{u}(k), \quad (16)$$

$$\mathbf{y}(k+1) = \overbrace{\begin{bmatrix} \hat{\mathbf{C}} \\ \mathbf{0} & \mathbf{C} & \mathbf{0} \end{bmatrix}}^{\hat{\mathbf{C}}} \boldsymbol{\chi}(k+1). \quad (17)$$

The augmented state is given by $\boldsymbol{\chi}(k) = [\Delta \mathbf{x}^T(k), \mathbf{x}^T(k), \Delta \mathbf{d}^T(k)]^T$ (for a general variable $b(k)$, $\Delta b(k) = b(k) - b(k-1)$, i.e., the Δ operator denotes the change in a variable between sample steps $k-1$ and k). Augmented state predictions can then be formed through iterative state substitution. This leads to the following matrices for state prediction:

$$\begin{bmatrix} \boldsymbol{\chi}(k+1) \\ \boldsymbol{\chi}(k+2) \\ \vdots \\ \boldsymbol{\chi}(k+N) \end{bmatrix} = \begin{bmatrix} \hat{\mathbf{A}} \\ \hat{\mathbf{A}}^2 \\ \vdots \\ \hat{\mathbf{A}}^N \end{bmatrix} \boldsymbol{\chi}(k) + \begin{bmatrix} \hat{\mathbf{B}} & & & \\ \hat{\mathbf{A}}\hat{\mathbf{B}} & \hat{\mathbf{B}} & & \\ \vdots & \vdots & \ddots & \\ \hat{\mathbf{A}}^{N-1}\hat{\mathbf{B}} & \dots & \dots & \hat{\mathbf{B}} \end{bmatrix} \begin{bmatrix} \Delta \mathbf{u}(k) \\ \Delta \mathbf{u}(k+1) \\ \vdots \\ \Delta \mathbf{u}(k+N-1) \end{bmatrix} \quad (18)$$

The predicted state $\tilde{\mathbf{x}}(k+1)$ and incremental predicted state $\Delta \tilde{\mathbf{x}}(k+1)$ can be found from these equations, where for a general vector \mathbf{p} , its prediction vector is $\tilde{\mathbf{p}}(k) = [\mathbf{p}^T(k), \dots, \mathbf{p}^T(k+H-1)]^T$, where H is called the prediction horizon

170 for the system.

It should be noted that once these predictions have been formed it is straightforward to consider the case where there is control communication delays. If there is a delay of ς samples, then $\Delta \mathbf{u}(k), \dots, \Delta \mathbf{u}(k+\varsigma-1)$ are considered constant at the values that they were calculated at in sample steps $k-\varsigma, \dots, k-1$, and input variables $\Delta \mathbf{u}(k+\varsigma), \dots, \Delta \mathbf{u}(k+H-1)$ are optimised for. Thus the input prediction matrices in (18) can be separated into those that correspond to the constant part of the input vector and the part that corresponds to the subset of the predicted inputs that are to be optimised for.

MPC problems are constructed to fulfill control objectives for a system based on knowledge of $\chi(k)$. A cost function, $J(\chi(k), \Delta\tilde{\mathbf{u}}(k))$ (which will henceforth be denoted by $J(k)$), is designed so as to embody the system's objectives. One of the major advantages of MPC is its ability to explicitly impose constraints in the formulation of the control problem. In some cases constraints associated with the MPC may be violated such that the MPC problem will be non-feasible. It is possible to 'soften' these constraints using an additional slack variable, ϵ , such that feasibility is guaranteed. In this case the MPC problem is given as follows [34]:

$$\min_{\Delta\tilde{\mathbf{u}}(k), \epsilon} J(k) + \rho\epsilon \quad (19)$$

$$\text{such that } \Gamma\Delta\tilde{\mathbf{u}}(k) \leq \mathbf{b}_I + \mathbf{1}\epsilon,$$

where Γ and \mathbf{b}_I are the inequality constraint matrix and vector, respectively, $\mathbf{1}$ is a vector of 1's with the same dimensionality as \mathbf{b}_I , and ρ is a weight which determines the degree to which the inequality constraint is satisfied in relation to $J(k)$.

Once $\Delta\tilde{\mathbf{u}}(k)$ has been calculated, then the value $\Delta\mathbf{u}(k)$ is applied to the system such that $\mathbf{u}(k) = \mathbf{u}(k-1) + \Delta\mathbf{u}(k)$. The MPC process is then carried out each sample step, using the updated state and looking one step further in the so-called "rolling horizon" fashion.

3.2. State estimation using Kalman filtering

When states and disturbances for MPC are unmeasurable a Kalman filter must be used to estimate them. Kalman filters allow a maximum likelihood estimate of states to be formed provided the noise associated with both the states and the output measurements are normally distributed about the mean [35]. It effectively combines the current output measurement with the predicted state measurement to provide an updated estimation of the current state estimate. We will henceforth assume that Kalman filtering is used with MPC for the rest of the paper to estimate unmeasured and unknown states and disturbances.

As the state and disturbance are estimated in this paper the following state-

space matrix is used for Kalman filter state and disturbance estimates:

$$\overbrace{\begin{bmatrix} \mathbf{x}_\epsilon(k+1) \\ \mathbf{d}_\epsilon(k+1) \end{bmatrix}}^{\boldsymbol{\chi}_\epsilon(k+1)} = \overbrace{\begin{bmatrix} \mathbf{A} & \mathbf{D} \\ \mathbf{0} & \mathbf{I} \end{bmatrix}}^{\mathbf{A}_\epsilon} \boldsymbol{\chi}_\epsilon(k) + \overbrace{\begin{bmatrix} \mathbf{B} \\ \mathbf{0} \end{bmatrix}}^{\mathbf{B}_\epsilon} \mathbf{u}(k), \quad (20)$$

where \mathbf{x}_ϵ and \mathbf{d}_ϵ are state and disturbance estimates, respectively, $\boldsymbol{\chi}_\epsilon(k)$ is the current Kalman filter state and disturbance estimation vector, and \mathbf{A}_ϵ and \mathbf{B}_ϵ are the associated state estimation matrices. Consider the following output measurement,

$$\mathbf{z}(k) = \mathbf{y}(k) + \mathbf{v}(k) = \mathbf{C}_\epsilon \boldsymbol{\chi}(k) + \mathbf{v}(k), \quad (21)$$

where $\mathbf{v}(k) \sim \mathcal{N}(0, \boldsymbol{\sigma}_v)$, where $\boldsymbol{\sigma}_v$ is the covariance at sample step k of the output measurement, and \mathbf{C}_ϵ is the Kalman state output matrix. A Kalman filter effectively merges the predicted state measurement from (20) with the new output measurement given by (21), to give an update of the new state estimate and the associated state covariance matrix $\mathbf{P}(k)$ as follows [36]:

$$\mathbf{P}^*(k) = \mathbf{A}_\epsilon \mathbf{P}(k) \mathbf{A}_\epsilon^\top + \boldsymbol{\sigma}_w, \quad (22)$$

$$\mathbf{K}(k+1) = \mathbf{P}^*(k) \mathbf{C}_\epsilon^\top (\mathbf{C}_\epsilon \mathbf{P}^*(k) \mathbf{C}_\epsilon^\top + \boldsymbol{\sigma}_v)^{-1}, \quad (23)$$

$$\begin{aligned} \boldsymbol{\chi}_\epsilon(k+1) &= (\mathbf{I} - \mathbf{K}(k+1) \mathbf{C}_\epsilon) (\mathbf{A}_\epsilon \boldsymbol{\chi}(k) + \mathbf{B}_\epsilon \mathbf{u}(k)) \\ &\quad + \mathbf{K}(k+1) \mathbf{z}(k), \end{aligned} \quad (24)$$

$$\mathbf{P}(k+1) = (\mathbf{I} - \mathbf{K}(k+1) \mathbf{C}_\epsilon) \mathbf{P}^*(k), \quad (25)$$

where $\mathbf{P}^*(k+1)$ is the covariance as predicted by (20). The Kalman gain matrix \mathbf{K} is chosen on the basis of the error covariance and noise statistics at sample step $k-1$, so as to minimise the variance of the next estimate. When the Kalman filter is used with MPC $\mathbf{x}(k) = \mathbf{x}_\epsilon(k)$, and $\mathbf{d}(k) = \mathbf{d}_\epsilon(k)$.

200 4. The application of MPC for AGC, and details of the Dome toolbox implementation

4.1. Deriving the state-space MPC model from the semi-implicit DAE.

The first step involved in designing the MPC is to derive a suitable state-space model that considers the dynamics of the system at the time-scales of

205 interest. The authors have developed custom functionality for the ‘Dome’ power systems simulation package [27] that automates the process whereby the state-space matrix used for control is constructed. This process will now be described.

The dynamic behaviour of electrical power systems can be described using a nonlinear semi-implicit differential algebraic equation (SIDAE) [37]:

$$\begin{bmatrix} \mathbf{T}_{\text{nl}} & \mathbf{0} \\ \mathbf{R}_{\text{nl}} & \mathbf{0} \end{bmatrix} \begin{bmatrix} \dot{\mathbf{x}}_{\text{nl}} \\ \mathbf{0} \end{bmatrix} = \begin{bmatrix} \mathbf{f}(\mathbf{x}_{\text{nl}}, \mathbf{y}_{\text{nl}}) \\ \mathbf{g}(\mathbf{x}_{\text{nl}}, \mathbf{y}_{\text{nl}}) \end{bmatrix} \quad (26)$$

where \mathbf{x}_{nl} denotes the dynamic states of the nonlinear power system, \mathbf{y} are the algebraic states, and in general \mathbf{T}_{nl} and \mathbf{R}_{nl} are time-variant, non-diagonal and non-full rank. The matrix $\mathbf{0}$ denotes a matrix of zeros. Equations \mathbf{f}_{nl} are the explicit part of the nonlinear differential equations and \mathbf{g}_{nl} are the explicit part of the nonlinear algebraic equations. The first step to deriving the state-space matrices used by MPC is to linearise (26) giving:

$$\begin{bmatrix} \hat{\mathbf{T}} & \mathbf{0} \\ \hat{\mathbf{R}} & \mathbf{0} \end{bmatrix} \begin{bmatrix} \dot{\mathbf{x}}_{\text{nl}} \\ \mathbf{0} \end{bmatrix} = \begin{bmatrix} \mathbf{f}_x & \mathbf{f}_y \\ \mathbf{g}_x & \mathbf{g}_y \end{bmatrix} \begin{bmatrix} \mathbf{x}_l \\ \mathbf{y} \end{bmatrix}, \quad (27)$$

where $\hat{\mathbf{T}}$, $\hat{\mathbf{R}}$, \mathbf{f}_x , \mathbf{f}_y , \mathbf{g}_x , and \mathbf{g}_y are the linearisations of \mathbf{T}_{nl} , \mathbf{R}_{nl} , $\mathbf{f}(\mathbf{x}_{\text{nl}}, \mathbf{y})$, and $\mathbf{g}(\mathbf{x}_{\text{nl}}, \mathbf{y})$ with respect to the \mathbf{x}_{nl} and \mathbf{y}_0 at linearisation point $(\mathbf{x}_{\text{nl}0}, \mathbf{y}_0)$.

210 The linearised state variables are given by $\mathbf{x}_l = \mathbf{x}_{\text{nl}} - \mathbf{x}_{\text{nl}0}$ and the linearised algebraic variables are given by $\mathbf{y} = \mathbf{y}_{\text{nl}} - \mathbf{y}_0$. At this stage (27) represents a linearisation of the entire simulated system. The following paragraphs show how the state-space used for control is extracted from this linearised semi-implicit model of the system.

The MPC typically has access to the models and inputs of a subset of devices for the purposes of control, and so these first must be separated from the remaining elements in the system. The dynamic states, the equations relevant to the MPC, and the inputs are expressed separately from the remaining system states, algebraic variables, and dynamic equations as follows:

$$\begin{bmatrix} \mathbf{T} & \mathbf{T}_{\text{xg}} & \mathbf{0} & \mathbf{0} \\ \mathbf{T}_{\text{rxd}} & \mathbf{T}_{\text{rxg}} & \mathbf{0} & \mathbf{0} \\ \mathbf{R} & \mathbf{R}_{\text{xg}} & \mathbf{0} & \mathbf{0} \\ \mathbf{R}_{\text{rxd}} & \mathbf{R}_{\text{rxg}} & \mathbf{0} & \mathbf{0} \end{bmatrix} \begin{bmatrix} \dot{\mathbf{x}}_{\text{d}} \\ \dot{\mathbf{x}}_{\text{g}} \\ \mathbf{0} \\ \mathbf{0} \end{bmatrix} = \begin{bmatrix} \mathbf{f}_{\text{xd}} & \mathbf{f}_{\text{xg}} & \mathbf{f}_y & \mathbf{f}_u \\ \mathbf{f}_{\text{rxd}} & \mathbf{f}_{\text{rxg}} & \mathbf{f}_{\text{ry}} & \mathbf{f}_{\text{ru}} \\ \mathbf{g}_x & \mathbf{g}_{\text{xg}} & \mathbf{g}_y & \mathbf{g}_u \\ \mathbf{g}_{\text{rxd}} & \mathbf{g}_{\text{rxg}} & \mathbf{g}_{\text{ry}} & \mathbf{g}_{\text{ru}} \end{bmatrix} \begin{bmatrix} \mathbf{x}_{\text{d}} \\ \mathbf{x}_{\text{g}} \\ \mathbf{y}_{\text{r}} \\ \mathbf{u} \end{bmatrix} \quad (28)$$

215 Here \mathbf{x}_d denotes the dynamic states which the MPC has access to for use in
its model. The remaining states which are not used by MPC are denoted by
 \mathbf{x}_g . The control inputs, \mathbf{u} , used for AGC are considered as algebraic variables.
Thus, these are separated from the remaining algebraic variables \mathbf{y}_r . The first
and third rows of (28) (the rows corresponding to \mathbf{T} and \mathbf{R}) denote the rows of
220 dynamic and algebraic equations which the MPC has access to. The second and
fourth rows of equations are used in the simulation but are not known by the
MPC. As it is assumed that \mathbf{x}_g is unknown to the MPC, then the MPC model
ignores the effects of matrices \mathbf{f}_{xg} and \mathbf{g}_{xg} .

This leaves the following two equations which can be used to form the state-
space representation:

$$\begin{bmatrix} \mathbf{T} & \mathbf{0} \\ \mathbf{R} & \mathbf{0} \end{bmatrix} \begin{bmatrix} \dot{\mathbf{x}}_d \\ \mathbf{0} \end{bmatrix} = \begin{bmatrix} \mathbf{f}_x & \mathbf{f}_u & \mathbf{f}_y \\ \mathbf{g}_x & \mathbf{g}_u & \mathbf{g}_y \end{bmatrix} \begin{bmatrix} \mathbf{x}_d \\ \mathbf{u} \\ \mathbf{y}_r \end{bmatrix} \quad (29)$$

By rearranging the second row of (29) to give \mathbf{y}_r in terms of \mathbf{x}_d , \mathbf{u} , and $\dot{\mathbf{x}}_d$, and
225 substituting this value of \mathbf{y}_r into the first row of (29), the state-space represen-
tation $\dot{\mathbf{x}}_d = \mathbf{A}_d \mathbf{x}_d + \mathbf{B}_d \mathbf{u}$ can be found where $\mathbf{A}_d = (\mathbf{T} - \mathbf{f}_y \mathbf{g}_y^{-1} \mathbf{R}_x)^{-1} (\mathbf{f}_x - \mathbf{f}_y \mathbf{g}_y^{-1} \mathbf{g}_x)$
and $\mathbf{B}_d = (\mathbf{T} - \mathbf{f}_y \mathbf{g}_y^{-1} \mathbf{g}_x)^{-1} (\mathbf{f}_u - \mathbf{f}_y \mathbf{g}_y^{-1} \mathbf{g}_u)$.

Often the dynamics of certain states of the MPC state-space model will
occur on time-scales which are relatively fast in comparison to the dynamics of
the other states. By considering these variables as algebraic in the MPC state-
space model, it allows larger sample times to be used for the discretisation of
the model. As a result the MPC can predict the system response further into
the future for the same prediction horizon. This is conducted as follows. The
dynamic states are divided into those states whose dynamics are maintained,
 \mathbf{x} , and those whose time constants are to be set to zero \mathbf{x}_0 . Setting the time
constants associated with \mathbf{x}_0 to zero gives the following:

$$\begin{bmatrix} \dot{\mathbf{x}} \\ \mathbf{0} \end{bmatrix} = \overbrace{\begin{bmatrix} \mathbf{A}_{11} & \mathbf{A}_{12} \\ \mathbf{A}_{21} & \mathbf{A}_{22} \end{bmatrix}}^{\mathbf{A}_d} \begin{bmatrix} \mathbf{x} \\ \mathbf{x}_0 \end{bmatrix} + \overbrace{\begin{bmatrix} \mathbf{B}_1 \\ \mathbf{B}_2 \end{bmatrix}}^{\mathbf{B}_d} \mathbf{u} \quad (30)$$

Then by expressing \mathbf{x}_0 in terms of \mathbf{x} and \mathbf{u} using the second row of the (30) the state-space representation to be used for the control of the system is given by:

$$\dot{\mathbf{x}}(t) = \mathbf{A}\mathbf{x}(t) + \mathbf{B}\mathbf{u}(t), \quad (31)$$

where $\mathbf{A} = \mathbf{A}_{11} - \mathbf{A}_{12}\mathbf{A}_{22}^{-1}\mathbf{A}_{21}$ and $\mathbf{B} = \mathbf{B}_1 - \mathbf{A}_{12}\mathbf{A}_{22}^{-1}\mathbf{B}_2$. Having discussed how the MPC state-space is formed from the nonlinear SIDAE, the constitution
 230 of the state-space model and the construction of the MPC cost function and constraints are now outlined.

4.2. Implementation of MPC for AGC

In this section it is outlined how the MPC is used to perform AGC. In this paper the MPC has access to the dynamic state equations of the synchronous
 235 generators responsible for providing AGC, as given by (1)-(6). As (3)-(6) typically have time constants significantly faster than those in (1) and (2), the time constants in (3)-(6) are set to 0 such that these equations are considered algebraic, for the purposes of the state-space modelling for control. Similarly, the time constants of states associated with the AVR and PSS dynamics are set to
 240 zero. Then the algebraic values of these variables are incorporated into (1) and (2) using straightforward matrix manipulation. These assumptions have been made previously for MPC in [9], and for Kalman filtering in [22]. In turn by zeroing these faster dynamics in the state-space representation for the control, it allows larger sample times to be used for the discretisation of the state-space
 245 for control and estimation. TSOs can then use PMU measurements of the frequency and rotor position to infer the other unknown states using the Kalman filter.

The \mathbf{A} and \mathbf{B} matrices are derived by applying a Zero Order Hold discretisation to their equivalent continuous-time matrices. The state vector, $\mathbf{x}(k) =$
 250 $[\mathbf{x}_1^T, \dots, \mathbf{x}_{n_g}^T]^T$, where n_g denotes the number of synchronous generators in the system. The synchronous generator state $\mathbf{x}_i = [\delta_i, \omega_i, x_{g1i}, x_{g2i}, x_{g3i}]^T$, is considered by the MPC, with x_{g1i}, x_{g2i} and x_{g3i} denoting the turbine states for generator i . Here, the measurement vector $\mathbf{z}(k) = [\mathbf{z}_1^T, \dots, \mathbf{z}_{n_g}^T]^T$, with $\mathbf{z}_i = [\delta_i, \omega_i]^T$.

The input vector is given by $\mathbf{u} = [p_{\text{order},\mathcal{W}\{1\}}(k), \dots, p_{\text{order},\mathcal{W}\{n_{\text{gu}}\}}(k)]^T$, for
255 $i \in \mathcal{W}$. Here, \mathcal{W} denotes the ordered set of synchronous generators that contribute to AGC, with cardinality n_{gu} . The disturbances are given by $\mathbf{d}(k) = [d_1, \dots, d_{n_{\text{g}}}]^T$, and represent the observed difference between $\omega_i(k)$, and its predicted value at sample step $k - 1$, for $i \in 1, \dots, n_{\text{g}}$. Thus the \mathbf{D} matrix is
260 given by a matrix of zeros, with ones placed such that the elements of $\mathbf{d}(k)$ are added to the relevant $\boldsymbol{\omega}(k)$'s. It is necessary for the control agent to receive the measurement vector $\mathbf{z}(k)$ from the generators, then perform state estimation, calculate the control inputs, and then send the setpoints to each of the generators. Thus, this will incur communication delays which can be factored into the MPC calculations as described in Section 3.

The cost function was chosen so as to represent the desire to minimise frequency deviations from ω_{s} , the Rate Of Change Of Frequency (ROCOF), and the financial costs associated with the control. An additional stabilising cost was added to minimise the rate of change of input $\Delta\mathbf{u}(k)$. The final cost function is given by:

$$J_{\text{agc}}(k) = \tilde{\mathbf{e}}_{\omega}^T(k+1)\mathbf{Q}_{e_{\omega}}\tilde{\mathbf{e}}_{\omega}(k+1) + \Delta\tilde{\mathbf{u}}^T(k)\mathbf{Q}_{\mathbf{u}}\Delta\tilde{\mathbf{u}}(k) \quad (32)$$

$$+ \Delta\tilde{\mathbf{w}}^T(k+1)\mathbf{Q}_{\omega}\Delta\tilde{\mathbf{w}}(k+1) + \Delta\tilde{\mathbf{p}}(k+1)^T\mathbf{Q}_{\mathbf{p}}\Delta\tilde{\mathbf{p}}(k+1),$$

265 where $\mathbf{e}_{\omega}(k) = \mathbf{C}_{\omega}\boldsymbol{\chi}(k) - \mathbf{1} = [\omega_1(k) - 1, \dots, \omega_{n_{\text{g}}}(k) - 1]^T$, $\Delta\mathbf{w}(k) = \mathbf{C}_{\Delta\omega}\boldsymbol{\chi}(k) = [\Delta\omega_1(k), \dots, \Delta\omega_{n_{\text{g}}}(k)]^T$, and $\Delta\mathbf{p}(k) = \mathbf{C}_{\Delta p}\boldsymbol{\chi}(k) = [\Delta p_{\text{m}\mathcal{W}\{1\}}(k), \dots, \Delta p_{\text{m}\mathcal{W}\{n_{\text{gu}}\}}(k)]^T$, where $p_{\text{mi}}(k)$ is the output power injected into the system by the i^{th} turbine generator at sample step k . The vector $\mathbf{1} \in \Re^{1 \times n_{\text{g}}}$ is a vector of ones, and the matrices \mathbf{C}_{ω} , $\mathbf{C}_{\Delta\omega}$, and $\mathbf{C}_{\Delta p}$ are matrices of zeros with entries
270 of 1 such that the equalities in the previous sentence hold. The financial costs are minimised by making the diagonal entries of $\mathbf{Q}_{\mathbf{p}}$ proportional to the costs associated with the generator power. Thus the controller will be less inclined to use generators with larger costs. It should be noted that it is possible to regulate tie line interconnectors using MPC such that they are maintained at
275 their scheduled values, as in [18], but this is not considered in this paper.

It is desired to maintain the constraints associated with the input to the

turbine governor as shown in Fig. 1. As ω_i is affected by disturbances that could result in feasibility issues for the MPC, this constraint is ‘softened’ in the MPC formulation using a slack constraint variable ϵ , as follows [34]:

$$\begin{aligned} \Delta \tilde{\mathbf{u}}^*(k) &= \min_{\Delta \tilde{\mathbf{u}}(k), \epsilon} J(k) + \rho \epsilon, \\ \text{s.t.} \quad \begin{bmatrix} \tilde{\mathbf{p}}_{ini}(k+1) \\ -\tilde{\mathbf{p}}_{ini}(k+1) \end{bmatrix} &\leq \begin{bmatrix} \mathbf{p}_{ini,\max} \\ -\mathbf{p}_{ini,\min} \end{bmatrix} + \mathbf{1}\epsilon, \quad \forall i \in \mathcal{W}, \\ \epsilon &\geq 0, \end{aligned} \quad (33)$$

where $p_{ini}(k) = R^{-1}(\omega_s - \omega_i(k)) + u_i(k)$, $\mathbf{p}_{ini,\max} = [p_{ini,\max}, \dots, p_{ini,\max}]^T$, $\mathbf{p}_{ini,\min} = [p_{ini,\min}, \dots, p_{ini,\min}]^T$, where $p_{ini,\max}$ and $p_{ini,\min}$ are the maximum and minimum constraints on p_{ini} , respectively, and $\mathbf{1}$ is a column of 1’s. The inclusion of this constraint improves the ability of the MPC to predict how the system will evolve over time, and so improves the overall frequency tracking performance. Once the state matrices and cost function have been defined, then the Kalman filter and MPC operate each time step, as outlined in Section 3.

The authors have developed integrated MPC and Kalman filtering functionality for the Dome simulation package. This automates the process of building the MPC and Kalman filter once the desired system states and inputs for use in system control have been identified. Once these have been chosen Dome extracts the state-space model accordingly. For the purposes of the quadratic optimisation routine, a custom built C interface to the Gurobi [33] optimisation package was developed to maximise the efficiency with which the optimisation routine could be called.

A dedicated wrapper function **MPCAGC** acts as an interface to the MPC and Kalman filtering functionality to implement AGC in the Dome simulation package. As arguments this function takes the various tunable parameters such as the cost function weights and prediction horizon as input. This significantly simplifies the process of applying MPC to large power systems, and can reduce considerably the typical effort involved in prototyping an MPC control system for an arbitrary power system.

It is assumed in the above that TSOs have accurate models of generator

responses. Typically, it will be necessary for generators to provide TSOs with
300 suitably accurate models of the plants such that TSOs can accurately simulate
the power system. Even if these are provided as black boxes TSOs could po-
tentially use system identification techniques in order to determine generator
models for use in the state-space. In the remainder of the paper it is assumed
that the simulation and control models of generators are equivalent.

305 5. Case Study

In this section, a modified version of the Irish transmission system grid is
used in order to evaluate the performance of the MPC based control system
against the PI controller. The Irish Transmission system grid, which has been
made available by Eirgrid, the Irish TSO, to researchers in the authors' research
310 group, consists of 1,479 buses, 1,851 transmission lines and transformers, 245
loads, 22 conventional synchronous power plants modelled with 6th order syn-
chronous machine models with AVRs and turbine governors, 6 PSSs, and 176
wind power plants, of which 142 are DFIGs and 34 CSWTs. This original un-
modified model provides a dynamic representation of the Irish electrical grid
315 which is topologically accurate and closely approximates the dynamics of the
actual Irish grid.

The aim of this paper is to compare the performance of MPC and PI based
AGC on this grid, when there is a large renewables penetration. Thus, the
authors have replaced 10 of the synchronous generators with wind turbines of
320 either DFIG or CSWT variety, on a like for like locational basis, using the same
PQ injections from the original load flow to give a renewables penetration of
55% (1.2 GW wind generation of 2.2 GW total active power generation). Of
the 13 remaining synchronous generators, 11 are used for AGC.

To evaluate the performance differences between the MPC and PI controllers,
325 two different simulation scenarios are considered. The first case, the nominal
case, is based on the loss of the largest infeed. This scenario is used to tune con-
trollers. Thus, firstly the AGC for both the MPC and PI controllers are tuned

so as to provide a fast and damped response when only this disturbance is considered, and when there is deterministic PQ loads. This tuning was performed
330 using trial and error, but this reflects the reality of how control algorithms are typically tuned in an industrial context. Effectively, the PI and MPC frequency regulation gains were raised until such time that the frequency, upon returning towards the 1 pu Hz setpoint would not overshoot the setpoint again. This first tuning case represents a case where there are some disturbances on the system
335 in the form of the loss of the largest infeed, some noise from wind generation, and the system nonlinearities.

The second scenario considers the effect of additional disturbances and model uncertainty on controller performance. The loss of the largest infeed scenario is considered again, except there are extra disturbances applied to the system
340 simultaneously. Typically, in the Irish grid when there is a large ROCOF in the system it causes the tripping of a number of wind farms, so the tripping of 5 wind turbines on the grid is simulated as occurring immediately after the loss of the largest infeed. Additionally, a transmission line is tripped, and the PQ loads are simulated in a stochastic fashion using Ornstein-Uhlenbeck processes
345 [31]. Finally, before the loss of the largest infeed, communication loss occurs between one of the generators that contribute to AGC and the TSO responsible for coordinating AGC. In both PI and MPC cases the controllers do not sense the communication loss and so they must be resilient to the model uncertainty. We simply refer to this as the *noise case* henceforth.

350 A sample time of 0.2 s is used for the MPC and the MPC is recalculated every 0.2 s. For the nominal and noise simulation scenarios, two different control delays are considered. In the first a minimum realistic delay of 0.2 s for the MPC (one sample step) is considered and compared to a PI control which experiences the same delay. Then in the second scenario, in order to evaluate
355 the performance of the controllers with a significant delay time, both controllers are compared when a 5 s communication delay is imposed. For the 0.2 s delay case the prediction horizon $H = 15$, and for the 5 s delay case $H = 39$. The MPC has a representation of all 13 synchronous generators for performing pre-

dictions as to how the system response will evolve and 11 of these generators
 360 participate in AGC. Thus the MPC models used $5 \times 13 = 65$ states for predic-
 tion, and optimises to calculate 11 inputs for the generators involved in AGC.
 State estimation and control are conducted as described in Section 4.

The following costs were allocated to the 11 generators, $[c_1, \dots, c_{11}] =$
 $[26.7, 26.7, 10, 26.7, \dots, 5, 2.5]$. The participation factors for use with the PI
 365 controller were found by finding the inverse of each of these costs and then nor-
 malising the participation factors such that the total equalled 1. The rationale
 here is that the cheapest power sources would have the largest participation
 factors and so the PI-based AGC would use more of these cheaper sources for
 frequency control.

370 All simulations are conducted using Dome. The Dome version utilized in
 this case study is based on Python 3.4.1; ATLAS 3.10.1 for dense vector and
 matrix operations; CVXOPT 1.1.8 for sparse matrix operations; and KLU 1.3.2
 for sparse matrix factorization. Gurobi [33] was used to perform the constrained
 optimisations for MPC. All simulations were executed on a ten core Intel Xeon
 375 processor with a speed of 2.2GHz, and running a 64-bit Linux OS.

5.1. Results

Firstly, the results for the 0.2 s communication delay are examined. Tun-
 ing based on this scenario results in a PI controller with an integral gain of
 $K_I = 10$. The MPC tuning results in gains of $\mathbf{Q}_{e\omega} = \text{diag}(1, \dots, 1)$, $\mathbf{Q}_\omega =$
 380 $\text{diag}(\alpha, \dots, \alpha)$, where α is repeated across the diagonal elements of \mathbf{Q}_ω , $\mathbf{Q}_u =$
 $\text{diag}(0.01, \dots, 0.01)$, and $\rho = 0.01$. The costs associated with generators deviat-
 ing from their setpoints, c_1, \dots, c_{11} , are incorporated into the cost function using
 the generator power weighting matrix, such that $\mathbf{Q}_p = 0.02 \times \text{diag}(c_1, \dots, c_{11})$.
 The resultant plot from the tuning scenario is given in Fig. 2. Here plots are
 385 given for MPC with $\alpha = 50$ and $\alpha = 0$, and finally the PI plot is given.

First of all it can be seen in Fig. 2 that the MPC with the desired tuning,
 with $\alpha = 50$, gives a highly damped response and outperforms the PI in terms
 of tightly regulating the frequency. Secondly, the MPC plots demonstrate the

effect of tuning α on MPC performance. By using a larger value of α it is possible
 390 to reduce the ROCOF and further reduce the initial frequency deviation. The
 MPC can be seen to offer significant improvements in terms of minimising the
 financial cost associated with control. In Fig. 3, it can be seen that the MPC
 uses more of the cheaper power source with cost $c_{10} = 5$, and less of the more
 expensive source with cost $c_1 = 26.7$, in comparison to the PI controller. This
 395 is because the MPC explicitly gives preference to the use of the least expensive
 generators. Finally, Fig. 4 illustrates the ability of the MPC to satisfy the
 slack constraint $p_{in11} \leq 1.02$ (note that Fig. 4 shows the input to the rate
 constraint before the rate constraint is applied). After the initial transient p_{in11}
 significantly exceeds the constraint. However, as discussed previously the use
 400 of the slack constraint maintains feasibility. The value of p_{in11} is then reduced
 such that it never significantly exceeds the constraint. The 0.2 s delay scenario
 is then run again for the noise case, as can be seen in Fig. 5. It can be seen here
 that the MPC provides significant robustness against uncertainty and provides
 tighter long term frequency regulation than the PI based controller when faced
 405 with the additional stochastic and model uncertainty. It has previously been
 noted in the literature that MPC results in improved robustness to disturbances
 when used for AGC [4, 20]. The MPC, however, does experience a slightly larger
 initial frequency nadir than the PI. It is assumed here that the initial increased
 frequency nadir for MPC is as a result of the particular model uncertainty faced
 410 by the MPC for the noise case, as the frequency nadirs were similar for both
 the PI and MPC with $\alpha = 50$ for the nominal case, as in Fig. 2.

The 5 s control communication delay scenario was then investigated in the
 same manner as the PI case. The same tuning used for the 0.2 s delay case is
 used again for the 5 s delay case, except $\mathbf{Q}_u = \text{diag}(0.03, \dots, 0.03)$ and $\alpha = 200$.
 415 It was necessary to detune these parameters, to achieve a damped response, as
 the parameters used in the 0.2 s delay case resulted in more oscillatory behaviour
 when used with the 5 s delay. The results of the tuning scenario can be seen
 in Fig. 6 and the noise scenario in Fig. 7. In both of these scenarios it is
 observed that, for the 5 s delay case, the MPC provides a negligible frequency

420 regulation improvement in comparison to the PI controller. The initial transient
has the largest impact on the frequency offset and, as MPC can predict how
this transient evolves, it is possible for it to take advantage of this response to
improve control performance. However, with a very long control delay the MPC
cannot take advantage of this transient and so the long delay time negates any
425 significant advantages posed by the MPC over the PI. However, the authors note
that the MPC is still capable of optimising the financial cost of providing control,
as can be seen in Fig. 8, where the MPC uses less of the expensive $c_1 = 26.7$
source, and more of the cheaper $c_{10} = 5$ source to provide the control. Thus, for
the case of the Irish grid presented here, from the perspective of providing tight
430 frequency regulation, it may not be worth installing MPC controllers instead
of PI controllers for frequency regulation unless suitably fast communication
links are in place first, so as to allow for tighter frequency control, as in the 0.2
s control delay scenarios. However, the MPC is still capable of providing the
control at a reduced financial cost for longer delays.

435 Finally, the time taken to calculate the MPC at each sample for the 5 s
delay, noise scenario case is given in Fig. 9. It is noted that the optimisation
time increases after 10 s as the inequality constraints in (33) become active. It
can be seen that the MPC is consistently calculated within the allocated sample
time of 0.2 s. Naturally the time taken using MPC will vary based on parameters
440 such as the sample time used, the prediction horizon, etc.

6. Conclusions and Future Work

The goal of this paper was to provide a means whereby the inefficiencies
inherent in the application of optimal control and estimation methods to large
scale electrical power system simulations could be overcome. As a demonstra-
445 tion, this paper evaluates the application of PI and Model Predictive Control
(MPC) when used for Automatic Generation Control (AGC) on a large-scale
Irish electrical grid model with a significant wind penetration and low inertia.
It was found that MPC could be used to provide tighter frequency regulation

than the PI controller for short control delays but did not provide a significant
450 improvement in frequency regulation for longer time delays. Thus it was noted
in the paper, that in order to gain full advantage from using MPC instead of
PI for AGC for frequency regulation for the case of the Irish grid, or other low
inertia grids, a fast communication network should first be installed. However,
in all delay cases the MPC was capable of reducing the costs associated with the
455 frequency regulation by explicitly considering the cost of the generation sources.
Potential future work on the themes in this paper could look at the application
of distributed optimal control methodologies across large scale realistic systems
such as the European grid and investigate further control issues such as non-
uniform control communication delays.

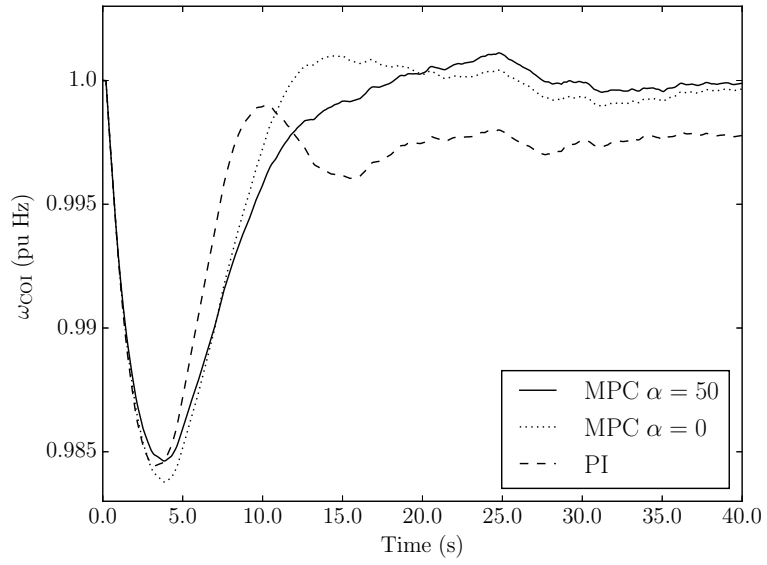


Figure 2: Frequency responses for nominal case with 0.2 s delay.

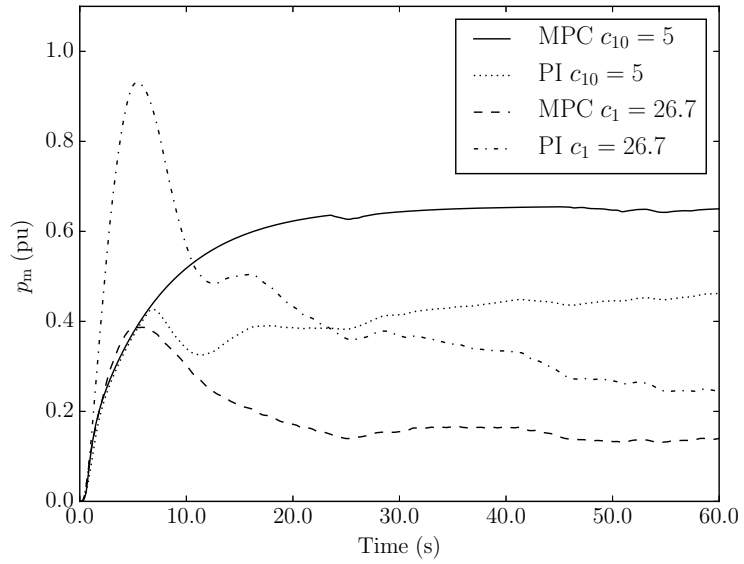


Figure 3: Generator power responses for nominal case with 0.2 s delay.

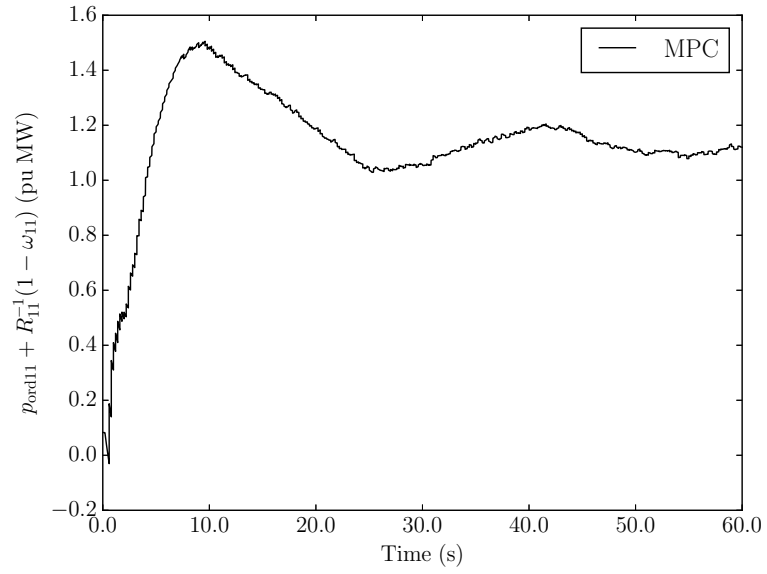


Figure 4: Satisfying p_{in} constraints at generator 11 for nominal case.

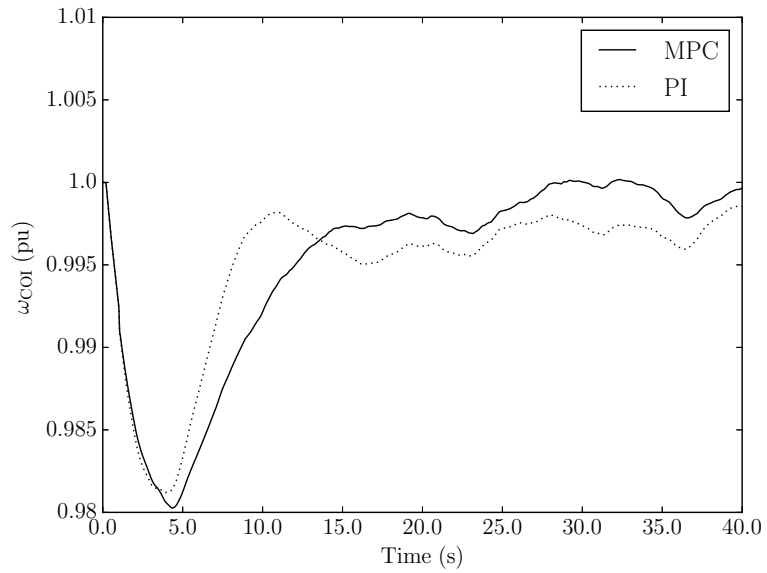


Figure 5: Frequency response under noise case with 0.2 s delay.

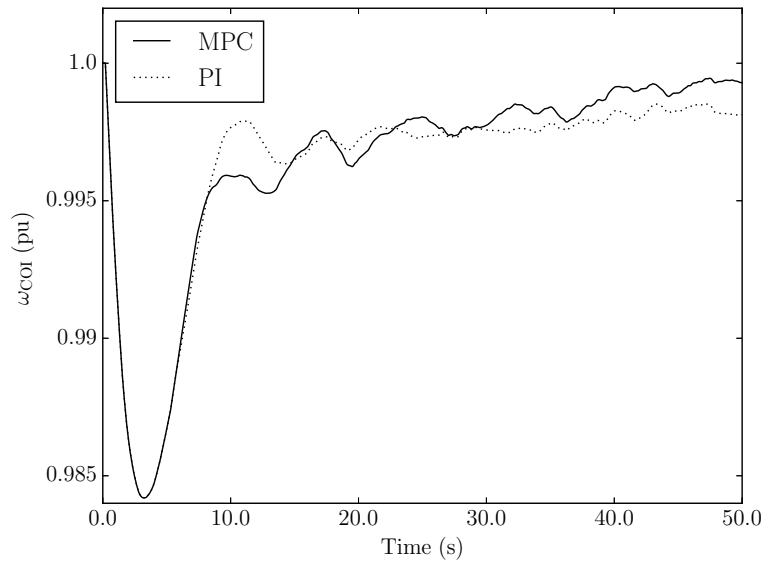


Figure 6: Frequency responses for nominal case with 5 s delay.

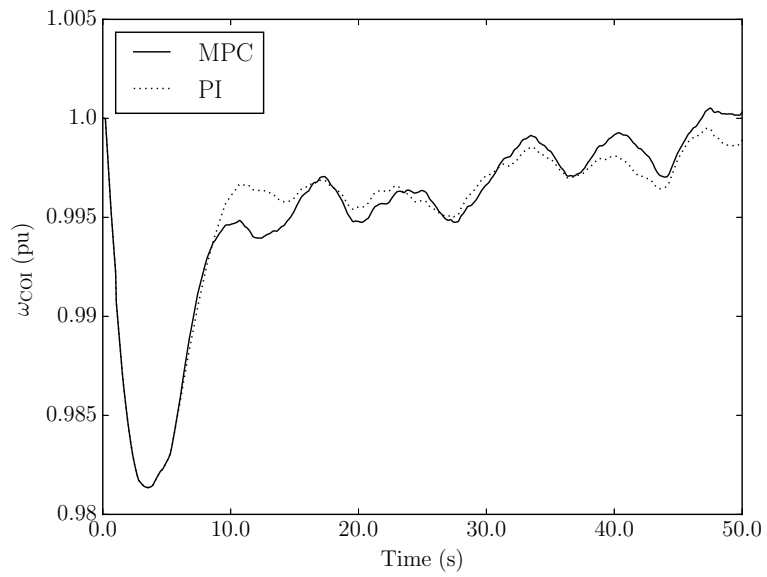


Figure 7: Frequency responses for noise case with 5 s delay.

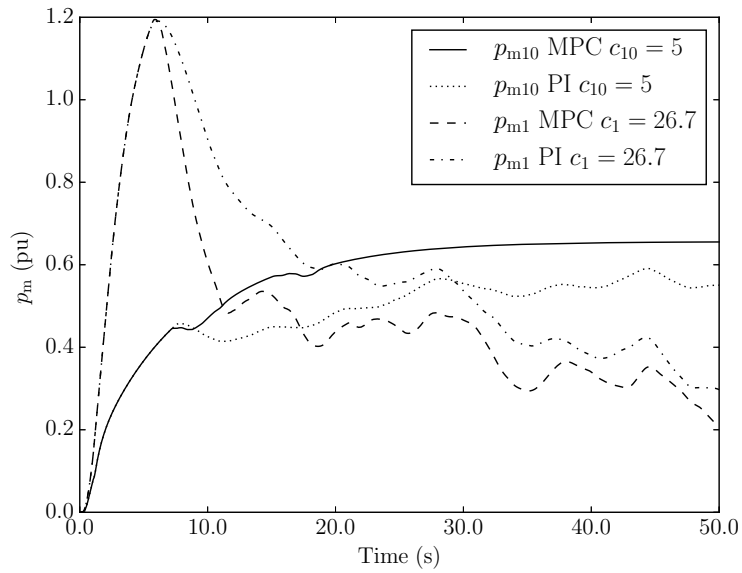


Figure 8: Mechanical power responses for noise case with 5 s delay.

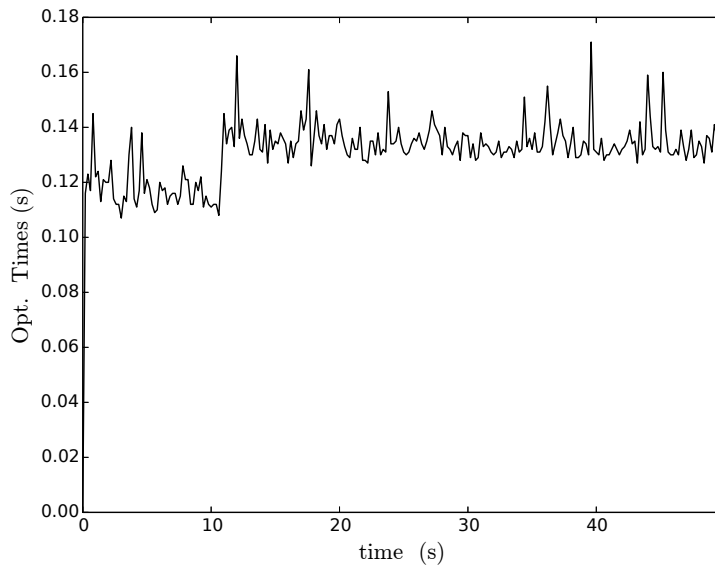


Figure 9: Optimisation times for noise case with 5 s delay simulation.

460 **Acknowledgment**

This material is based upon works supported by the Science Foundation Ireland, by funding Paul Mc Namara under Grant No. SFI/09/SRC/E1780, and Federico Milano under the Grant No. SFI/15/IA/3074. The opinions, findings and conclusions or recommendations expressed in this material are those of
465 the authors and do not necessarily reflect the views of the Science Foundation Ireland. Federico Milano is also funded by EC Marie Skłodowska-Curie Career Integration Grant No. PCIG14-GA-2013-630811.

- [1] P. W. Sauer and M. A. Pai, "Power system dynamics and stability," *Prentice Hall*, 1997.
- 470 [2] W. Winter, K. Elkington, G. Bareux, and J. Kostevc, "Pushing the limits: Europe's new grid: innovative tools to combat transmission bottlenecks and reduced inertia," *IEEE Power and Energy Magazine*, vol. 13, no. 1, pp. 60–74, 2015.
- 475 [3] R. Doherty, A. Mullane, G. Nolan, D. J. Burke, A. Bryson, and M. O'Malley, "An assessment of the impact of wind generation on system frequency control," *IEEE Transactions on Power Systems*, vol. 25, no. 1, pp. 452–460, 2010.
- 480 [4] P. Mc Namara, R. Meere, T. O'Donnell, and S. McLoone, "Control strategies for automatic generation control over MTDC grids," *Control Engineering Practice*, vol. 54, pp. 129–139, 2016.
- [5] J. L. Rodríguez-Amenedo, S. Arnalte, and J. C. Burgos, "Automatic generation control of a wind farm with variable speed wind turbines," *IEEE Transactions on Energy Conversion*, vol. 17, no. 2, pp. 279–284, 2002.
- 485 [6] E. F. Camacho and C. Bordons, *Model predictive control, 2nd Edition*. Springer, London, UK, 2003.

- [7] N. Li, C. Zhao, and L. Chen, “Connecting automatic generation control and economic dispatch from an optimization view,” *IEEE Transactions on Control of Network Systems*, vol. 3, no. 3, pp. 254–264, 2016.
- [8] C. Zhao, E. Mallada, S. Low, and J. Bialek, “A unified framework for frequency control and congestion management,” in *Proceedings of the Power Systems Computation Conference*, June 2016, pp. 1–7.
- [9] A. Ersdal, L. Imsland, and K. Uhlen, “Model predictive load-frequency control,” *IEEE Transactions on Power Systems*, vol. 31, no. 1, pp. 777–785, 2015.
- [10] M. Almassalkhi and I. Hiskens, “Model-predictive cascade mitigation in electric power systems with storage and renewables—part I: theory and implementation,” *IEEE Transactions on Power Systems*, vol. 30, no. 1, pp. 67–77, 2015.
- [11] A. Fuchs, M. Imhof, T. Demiray, and M. Morari, “Stabilization of large power systems using VSC–HVDC and model predictive control,” *IEEE Transactions on Power Delivery*, vol. 29, no. 1, pp. 480–488, 2014.
- [12] M. Moradzadeh, R. Boel, and L. Vandeveldel, “Voltage coordination in multi-area power systems via distributed model predictive control,” *IEEE Transactions on Power Systems*, vol. 28, no. 1, pp. 513–521, 2013.
- [13] A. Ulbig, T. Rinke, S. Chatzivasileiadis, and G. Andersson, “Predictive control for real-time frequency regulation and rotational inertia provision in power systems,” *52nd IEEE Conference on Decision and Control*, Firenze, Italy, pp. 2946–2953, 2013.
- [14] M. Shiroei, A.M. Ranjbar, “Supervisory predictive control of power system load frequency control,” *International Journal of Electrical Power & Energy Systems*, vol. 61, pp. 70–80, 2014.

- [15] P. Mc Namara, R. R. Negenborn, B. de Schutter, G. Lightbody, and S. McLoone, “Distributed MPC for frequency regulation in multi-terminal HVDC grids,” *Control Engineering Practice*, vol. 46, pp. 176–187, 2016.
- 515 [16] R. Hermans, A. Jokić, M. Lazar, A. Alessio, P. Van den Bosch, I. Hiskens, and A. Bemporad, “Assessment of non-centralised model predictive control techniques for electrical power networks,” *International Journal of Control*, vol. 85, no. 8, pp. 1162–1177, 2012.
- [17] A. Venkat, I. Hiskens, J. Rawlings, and S. Wright, “Distributed MPC
520 Strategies With Application to Power System Automatic Generation Control,” *IEEE Transactions on Control Systems Technology*, vol. 16, no. 6, pp. 1192–1206, Nov. 2008.
- [18] T.H. Mohamed, H. Bevrani, A.A. Hassan, and T. Hiyama, “Decentralized
525 model predictive based load frequency control in an interconnected power system,” *Energy Conversion and Management*, vol. 52, no. 2, pp. 1208–1214, 2011.
- [19] P. , Lampros, M.-S. Debry, T. Van Cutsem, and P. Panciatici, “Local control of AC/DC converters for frequency support between asynchronous AC
530 areas,” *Proceedings of the PowerTech 2017 Conference*, Manchester, UK, pp. 1–6, 2017.
- [20] T. H. Mohamed, J. Morel, H. Bevrani, and T. Hiyama, “Model predictive based load frequency control design concerning wind turbines,” *International Journal of Electrical Power & Energy Systems*, vol. 43, no. 1, pp. 859–867, 2012.
- 535 [21] F. Auger, M. Hilairet, J. M. Guerrero, E. Monmasson, T. Orłowska-Kowalska, and S. Katsura, “Industrial applications of the Kalman filter: A review,” *IEEE Transactions on Industrial Electronics*, vol. 60, no. 12, pp. 5458–5471, 2013.

- [22] X. Qin, B. Li, and N. Liu, “Dynamic State Estimator Based on Wide Area Measurement System During Power System Electromechanical Transient Process,” *Advanced Topics in Measurements*, p. 323, 2012.
- [23] E. Ghahremani and I. Kamwa, “Online state estimation of a synchronous generator using unscented Kalman filter from phasor measurements units,” *IEEE Transactions on Energy Conversion*, vol. 26, no. 4, pp. 1099–1108, 2011.
- [24] N. Zhou, D. Meng, Z. Huang, and G. Welch, “Dynamic state estimation of a synchronous machine using pmu data: A comparative study,” *IEEE Transactions on Smart Grid*, vol. 6, no. 1, pp. 450–460, 2015.
- [25] I. M. Sanz, “Control of AC/DC systems for improved transient stability and frequency support provision,” Ph.D. dissertation, Imperial College London, Feb. 2015. [Online]. Available: <https://spiral.imperial.ac.uk/handle/10044/1/25956>
- [26] J. A. Martin and I. A. Hiskens, “Corrective Model-Predictive Control in Large Electric Power Systems,” *IEEE Transactions on Power Systems*, vol. 32, no. 2, pp. 1651–1662, March 2017.
- [27] F. Milano, “A python-based software tool for power system analysis,” in *Proceedings of the IEEE PES General Meeting*, Vancouver, BC, Canada, July 2013, pp. 1–5.
- [28] —, *Power system modelling and scripting*. Springer Science & Business Media, 2010.
- [29] R. Zárate-Minano, F. M. Mele, and F. Milano, “SDE-based Wind Speed Models with Weibull Distribution and Exponential Autocorrelation,” Boston, MA, July 2016.
- [30] H. Louie, “Evaluation of probabilistic models of wind plant power output characteristics,” in *Proceedings of the International Conference on Probabilistic Methods Applied to Power Systems*, 2010, pp. 442–447.

- [31] F. Milano and R. Zárate-Miñano, “A systematic method to model power systems as stochastic differential algebraic equations,” *IEEE Transactions on Power Systems*, vol. 28, no. 4, pp. 4537–4544, 2013.
- 570 [32] P. Kundur, *Power System Stability and Control*. Mc-Graw Hill, New York, 1994.
- [33] Gurobi Optimization Inc., “Gurobi Optimizer Reference Manual,” 2015. [Online]. Available: <http://www.gurobi.com>
- [34] J. Maciejowski, *Predictive Control with Constraints*. Harlow, England: 575 Prentice Hall, 2002.
- [35] J. Rawlings and D. Mayne, *Model Predictive Control: Theory and Design*. Madison, Wisconsin: Nob Hill Publishing, 2009.
- [36] R. R. Labbe Jr., *Kalman and Bayesian filters in Python*, available online: robotics.itee.uq.edu.au/elec3004/2015/tutes/Kalman_and_Bayesian_Filters_in_Python.pdf, 2016. 580
- [37] F. Milano, “Semi-Implicit Formulation of Differential-Algebraic Equations for Transient Stability Analysis,” *IEEE Transactions on Power Systems*, vol. 31, no. 6, pp. 534–4543, 2016.